AIAA JOURNAL
Vol. 44, No. 9, September 2006

# Field Velocity Approach and Geometric Conservation Law for Unsteady Flow Simulations

Jayanarayanan Sitaraman* and James D. Baeder†
*University of Maryland at College Park, College Park, Maryland 20742*

DOI: 10.2514/1.5836

**A technique to model unsteady flow phenomenon which involves simultaneous elastic motions of the boundaries and interaction with gust fields is discussed. The field velocity approach is used to include the effect of the gust fields caused by a vortex wake into the flow computations. Elastic deformations of the boundaries cause changes in grid cell volumes which require the rigorous enforcement of the geometric conservation law. Mathematical modeling required to enforce conservation when performing such unsteady flow computations is presented. The application of the technique developed to a variety of problems from simple 2-D model problems to more complex realistic problems are described. The predictions obtained are validated with exact analytical results/experimental data as appropriate. Overall, the field velocity approach together with a technique to enforce the geometric conservation law is found to be a powerful tool for unsteady flow simulation.**

## Nomenclature

| | | |
|---|---|---|
| $C_n$ | = | normal force coefficient |
| $C_m$ | = | pitching moment coefficient |
| $C_T$ | = | thrust coefficient |
| $E$ | = | total energy |
| $H$ | = | total enthalpy |
| $J$ | = | Jacobian of transformation |
| $M$ | = | free stream Mach number |
| $q$ | = | flux vector |
| $u, v, w$ | = | aerodynamic velocity field |
| $u', v', w'$ | = | perturbation velocity field |
| $s$ | = | nondimensional time |
| $V$ | = | free stream velocity |
| $V_g$ | = | gust convection velocity |
| $x, y, z$ | = | Cartesian coordinates |
| $\lambda$ | = | speed ratio |
| $\mu$ | = | advance ratio |
| $\xi, \eta, \zeta$ | = | curvilinear coordinates |
| $\rho$ | = | density |
| $\sigma$ | = | solidity |
| $\tau$ | = | time in transformed coordinates |
| $\psi$ | = | azimuthal coordinate |

## I. Introduction

THE field velocity or grid velocity approach is a method for incorporating unsteady flow conditions via grid movement in computational fluid dynamic simulations. This approach provides a unique methodology for directly calculating aerodynamic responses to step changes in flow conditions. Physically, the grid velocity can be interpreted as the velocity of a grid point in the mesh during the unsteady motion of the boundary surface. For example, the simulation of a step change in angle of attack of an airfoil can be performed by incorporating a step change in vertical grid velocity all over the flow domain. This method effectively decouples the influence of pure angle of attack from that of a pitch rate because the airfoil is not made to pitch, and because the step change is enforced over the entire flow domain uniformly [1]. A similar methodology can be used for simulating responses of an airfoil to step changes in pitch rate and interaction with traveling vertical gusts or convecting vortices [2,3]. The grid velocity approaches are normally implemented without actually moving the grid. Rather, the time metrics are modified to effectively simulate the motion of the grid. But incorporation of the field velocity approach without actually moving the grid does at times violate the so-called geometric conservation law (especially when there is large variation in the grid velocities between successive grid points).

The geometric conservation law (GCL) is used to satisfy the conservative relations of the surfaces and volumes of the control cells in moving meshes. Primarily, the GCL states that the volumetric increment of a moving cell must be equal to the sum of the changes along the surfaces that enclose the volume. Thomas and Lombard [4] were the first to recognize the necessity of satisfying the geometric conservation laws simultaneously with other physical conservations when solving moving mesh problems. They proposed a differential form of the GCL which needs to be solved along with the conservative variables. More modern approaches [5–7] efficiently compute the space and time metrics in a manner that implicitly guarantees the satisfaction of the GCL.

One of the highly unsteady flow problems of practical interest is computing the flow field around a helicopter rotor blade undergoing aeroelastic deformations. The unsteadiness in flow field is primarily caused by the periodic blade motions and the wake induced inflow. Resorting to a global multiblock, overset mesh type approach (which models all the rotor blades) limits the practicality of such a calculation because of high computational overheads. Also one needs to carefully tune the grid spacings to preserve the trailed vortices. The use of a local single block approach (which models a single rotor blade) requires the inclusion of the influences of a trailed vortex wake, whose geometry is computed from using an external calculation (usually a Lagrangian vortex lattice approach [8]). The field velocity approach may be used for wake inclusion in such cases. In this approach, there is a dynamic real movement of the mesh because of the aeroelastic blade deformations and an apparent movement of the mesh because of the use of the field velocity approach [9]. This poses a unique challenge for preserving the GCL. The computation of space and time metrics should be performed consistently to maintain conservation and hence preserve accuracy.

The objectives of this research effort are threefold. The first objective is to demonstrate the capabilities of the grid velocity approach for the simulation of unsteady flow environments. The second objective is to develop methodologies for computing 4th order accurate space metrics and second order accurate time metrics

Presented as Paper 3835 at the 33rd AIAA Fluid Dynamics Conference and Exhibit, Orlando, Florida, 23–26 June 2003; received 15 October 2003; revision received 5 January 2006; accepted for publication 13 March 2006. 

*Assistant Research Scientist, Department of Aerospace Engineering.
†Associate Professor Associate, Department of Aerospace Engineering. Fellow AIAA.

which satisfy the geometric conservation law. Finally the methodologies developed will be applied to real helicopter rotor simulations and validated with flight test data in an effort to demonstrate the practical applicability.

## II. Methodology

The computations are performed using the extensively modified transonic unsteady rotor Navier—Stokes (TURNS) research code, which has been applied to a variety of helicopter problems [10–12]. A finite difference upwind numerical algorithm is used. In this algorithm, the evaluation of the inviscid fluxes is based on an upwind-biased flux-difference scheme originally suggested by Roe [13] and later extended to three-dimensional flows by Vatsa et al. [14]. The chief advantage of using upwinding is that it eliminates the addition of explicit numerical dissipation and has been demonstrated to produce less dissipative numerical solutions. This feature, coupled with a fine grid description in the tip region, increases the accuracy of the wake simulation. The Van Leer monotone upstream-centered scheme for conservation laws (MUSCL) approach is used to obtain third order accuracy, with Koren's differentiable flux limiters to make the scheme total variation diminishing.

The lower upper symmetric Gauss–Seidel (LU-SGS) scheme suggested by Jameson and Yoon [15,16] is used for the implicit operator. Briefly, the LU–SGS method is a direct modification of the approximate lower-diagonal-upper (LDU) factorization to the unfactored implicit matrix. The resulting factorization can be regarded as the symmetric Gauss–Seidel relaxation method. The LDU factorization yields better stability than the simple LU factorization because the diagonal elements always have the absolute value of the Jacobian matrices. Though the (LU–SGS) implicit operator increases the stability and robustness of the scheme, the use of a spectral radius approximation renders the method only first order accurate in time. Therefore, in this study a second order backwards difference in time is used, along with Newton-type subiterations to restore formal second order time accuracy.

Also the present numerical scheme employs a modified finite-volume method for calculating the metrics. Finite-volume formulations have the advantage that both the space and time metrics can be formed accurately and free stream is captured accurately [7]. Also it is to be noted that the computations include aeroelastic deformation and prescribed induced inflow variation. So, the space and time metrics need to be recomputed at each time step to maintain the required spatial and temporal accuracy. The computation of the space and time metrics will be discussed in detail in the following section.

## III. Calculation of Space and Time Metrics

The strong conservation-law form of the Navier–Stokes equations in Cartesian coordinates can be written as [17]

$$
\begin{gathered}
q_t + f_x + g_y + h_z = \sigma_x + \theta_y + \omega_z \\
q = (\rho, \rho u, \rho v, \rho w, \rho E)^T, \qquad E = e + \frac{u^2 + v^2 + w^2}{2} \\
f = (\rho u, p + \rho u^2, \rho uv, \rho uw, \rho uH)^T \\
g = (\rho v, \rho vu, p + \rho v^2, p + \rho vw, \rho vH)^T \\
h = (\rho w, \rho wu, \rho wv, p + \rho w^2, \rho wH)^T, \qquad H = E + p/\rho
\end{gathered}
\tag{1}
$$

where $u$, $v$, $w$ are the velocity components in the coordinate directions $x$, $y$, $z$; $\rho$ is the density, $p$ is the pressure, $e$ the specific internal energy; and $\sigma$, $\theta$, $\omega$ represent the viscous stress and work terms for each coordinate direction. Upon transforming to computational coordinates $\xi$, $\eta$, $\zeta$ with the aid of the chain rule of partial derivatives, Eq. (1) becomes

$$
\begin{gathered}
\hat{q}_\tau + \hat{f}_\xi + \hat{g}_\eta + \hat{h}_\zeta = \hat{\sigma}_\xi + \hat{\theta}_\eta + \hat{\omega}_\zeta, \qquad \hat{q} = Jq \\
\hat{f} = \hat{\xi}_t q + \hat{\xi}_x f + \hat{\xi}_y g + \hat{\xi}_z h, \qquad \hat{g} = \hat{\eta}_t q + \hat{\eta}_x f + \hat{\eta}_y g + \hat{\eta}_z h \\
\hat{h} = \hat{\zeta}_t q + \hat{\zeta}_x f + \hat{\zeta}_y g + \hat{\zeta}_z h, \qquad \hat{\sigma} = \hat{\xi}_x \sigma + \hat{\xi}_y \theta + \hat{\xi}_z \omega \\
\hat{\theta} = \hat{\eta}_x \sigma + \hat{\eta}_y \theta + \hat{\eta}_z \omega, \qquad \hat{\omega} = \hat{\zeta}_x \sigma + \hat{\zeta}_y \theta + \hat{\zeta}_z \omega
\end{gathered}
\tag{2}
$$

Here terms of form $\hat{\xi}_{x,y,z}$, $\hat{\eta}_{x,y,z}$ and $\hat{\zeta}_{x,y,z}$ are the space metrics, $\hat{\xi}_t$, $\hat{\eta}_t$ and $\hat{\zeta}_t$ are the time metrics in the computational domain, and $J$ is the Jacobian of the inverse coordinate transformation (i.e., $J = \det[\partial(x, y, z)/\partial(\xi, \eta, \zeta)]$).

### A. Field Velocity Approach

Mathematically, the field velocity approach can be explained by considering the velocity field, $V$, in the physical Cartesian domain. It can be written as

$$V = (u - x_\tau)i + (v - y_\tau)j + (w - z_\tau)k, \tag{3}$$

where $u$, $v$, and $w$ are components of the velocity along the coordinate directions and $x_\tau$, $y_\tau$, and $z_\tau$ are the corresponding grid time velocity component. For the flow over a stationary wing, these components are zero. For a rotor blade rotating about the $z$ axis, both $x_\tau$ and $y_\tau$ have nonzero values owing to the rotation of the mesh. Let the velocity induced by the external potential be represented by a velocity field $(u', v', w')$. Thus, the velocity field becomes

$$V = (u - x_\tau + u')i + (v - y_\tau + v')j + (w - z_\tau + w')k$$

The field velocity approach models this changed velocity field by changing the grid velocities. The modified grid velocities are defined as

$$\tilde{x_\tau} i + \tilde{y_\tau} j + \tilde{z_\tau} k = (x_\tau - u')i + (y_\tau - v')j + (z_\tau - w')k$$

Once the modified grid velocities are obtained, the grid time metrics in the computational domain $(\hat{\xi}_t, \hat{\eta}_t, \hat{\zeta}_t)$ are computed as

$$
\hat{\xi}_t = -\left(\hat{\xi}_x \tilde{x_\tau} + \hat{\xi}_y \tilde{y_\tau} + \hat{\xi}_z \tilde{z_\tau}\right), \qquad \hat{\eta}_t = -\left(\hat{\eta}_x \tilde{x_\tau} + \hat{\eta}_y \tilde{y_\tau} + \hat{\eta}_z \tilde{z_\tau}\right)
$$
$$
\hat{\zeta}_t = -\left(\hat{\zeta}_x \tilde{x_\tau} + \hat{\zeta}_y \tilde{y_\tau} + \hat{\zeta}_z \tilde{z_\tau}\right)
$$

### B. Geometric Conservation Law

The geometric conservation law (GCL) has the same form as the mass conservation law [first component of vector Eq. (2)] as it essentially represents the conservation of cell volumes. One can easily obtain the differential form of the GCL from the mass conservation equation by setting $\rho = 1$ and $V = (u, v, w) = 0$:

$$J_\tau + \left(\hat{\xi}_t\right)_\xi + \left(\hat{\eta}_t\right)_\eta + \left(\hat{\zeta}_t\right)_\zeta = 0 \tag{4}$$

The integral form of the GCL can be obtained in a similar manner and can be stated as

$$\nu(t_2) - \nu(t_1) = \int_{t_1}^{t_2} \oint_{S(t)} \boldsymbol{V}_s \cdot \boldsymbol{dS}\, \mathrm{d}t \tag{5}$$

where $\nu(t_2)$ and $\nu(t_1)$ are the initial and final volumes and $\boldsymbol{V}_s$ is the moving velocity of the cell surface. Equations (4) or (5) need to be satisfied in order to make the numerical discretization strictly conservative. Otherwise, artificial sources and sinks can be generated as a result of the numerical discretization. Thomas and Lombard [4] proposed the solution of Eq. (4) with the same differencing scheme as that used for solving the flow conservation equations to maintain the GCL. But this adds to the computational overhead of the calculation.

A more practical approach is to compute the Jacobian $J$ by its geometric definition and calculate the time metrics according to the geometric conservation law [7]. For example, for a first order

accurate time metric calculation one could find the time metrics in the computational domain as

$$\hat{\xi}_t = -\frac{V_{S^\xi}}{\Delta t}, \qquad \hat{\eta}_t = -\frac{V_{S^\eta}}{\Delta t}, \qquad \hat{\zeta}_t = -\frac{V_{S^\zeta}}{\Delta t}$$

Where $V_{S^\xi}$, $V_{S^\eta}$, and $V_{S^\zeta}$ are the volumes swept by the faces of the cell volume in the computational coordinate directions. This approach provides a methodology for implicitly satisfying the GCL without solving any additional equations. But, in a purely finite difference approach one is posed with the problem of identifying cell volumes. In other words, a strategy needs to be identified to define bounded volumes around mesh points which can be used for the computations of the Jacobian, space metrics and time metrics in a consistent manner.

### C. Defining Cell Volumes

To preserve the overall order of accuracy of the computations, the space and time metrics need to be calculated to the same order of accuracy as that of the underlying spatial and temporal numerical discretization. Using a classical finite difference approach, one calculates the transformation matrix $\partial(x, y, z)/\partial(\xi, \eta, \zeta)$ and inverts it to find the space metrics. The Jacobian of transformation is the determinant of this transformation matrix. The order of accuracy of the space metrics can be improved by using a larger finite difference stencil while evaluating individual terms of the above matrix. But, for surface conforming mesh geometries, it is possible to create overshoots and undershoots (e.g., at the trailing edge of an airfoil) when arbitrarily increasing the finite difference stencil, which causes divergence of the flow solution at times. Hence, a modified strategy, often referred to as the dual refined mesh approach [5], which computes the space metrics and Jacobian in a finite-volume like way is proposed.

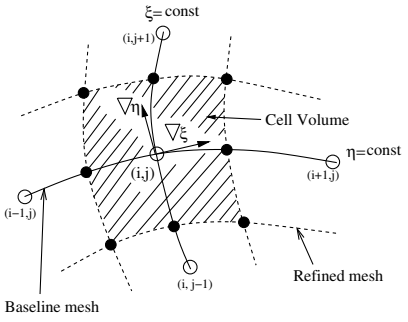


**a) Cell volume in two dimensions**

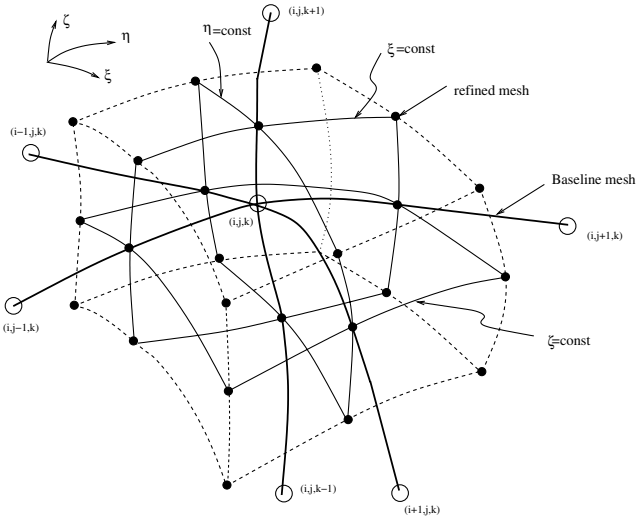


**b) Cell volume in three dimensions**

**Fig. 1 Definition of cell volumes.**

Figures 1a and 1b show the volumes around a mesh point for 2-D and 3-D, respectively. The open symbols represent the mesh points of the original mesh in which the computations of flow variables are performed. The closed symbols show the refined mesh generated by one dimensional interpolation in the direction of each of the computational coordinates. The refined mesh points are generated using a quartic monotone interpolation scheme proposed by Suresh and Hyunh [18]. The monotonicity of the interpolation scheme prevents the generation of overshoots and undershoots in the refined mesh geometry. Also, the fourth order interpolation makes the calculation of the Jacobians and space metrics 4th order accurate spatially, even though the computations of these are made in a finite-volume like way.

Once the refined mesh is obtained, a volume which is bounded by 24 faces (8 edges in 2-D) can be defined around the mesh point. The Jacobian of the transformation to the computational coordinates at every mesh point can be evaluated by consistently evaluating the volumes of these bounded cells. The Jacobian ($J$) in Eq. (2) is that of the inverse transformation and can be found by taking the inverse of the volumes calculated.

#### 1. *Evaluation of Space Metrics*

The space metrics are gradients to $\xi = \text{const}$, $\eta = \text{const}$, and $\zeta = \text{const}$ surfaces scaled by the Jacobian of inverse transformation. The definition of these surfaces are known from the refined mesh which was computed while defining the volumes. The gradients of these surfaces can be evaluated at every mesh point to find the space metrics.

For the computation of the right-hand side of the flow conservation equations in the discretized form, one often needs the space metrics at the interface points ($\xi = i \pm \frac{1}{2}$, $\eta = j \pm \frac{1}{2}$, $\zeta = k \pm \frac{1}{2}$). These are actually surface normals to the bounded cell defined around the mesh point (graphically described in Figs. 1a and 1b) which can be evaluated by computing the gradient vector to the appropriate surface.

#### 2. *Evaluation of Time Metrics*

The evaluation of the time metrics require computation of volumes swept by the faces of the bounded volume. The time metrics should have components resulting from both the actual deformation of the mesh and the external velocity field that is included using the field velocity approach. The methodology used for computations is illustrated in Fig. 2. The time metric in a particular computational coordinate direction is calculated by accumulating the volume swept by the face because of actual deformation and the apparent volume swept because of the field velocity components.

The temporal order of accuracy can be improved by using the volumes swept at previous time steps and devising an appropriate backward difference stencil (similar to the flow equations). To make the scheme strictly conservative, the Jacobian is recalculated by including the change in volume because of the apparent contribution from the field velocity components. The space metrics are still evaluated as surface normals to the actual deformed mesh, although

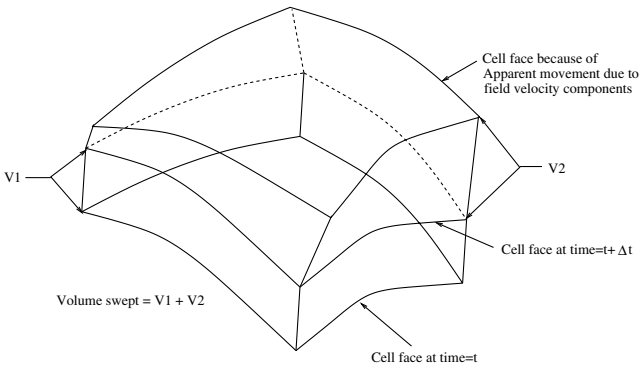


**Fig. 2 Evaluation of volumes swept by cell faces.**

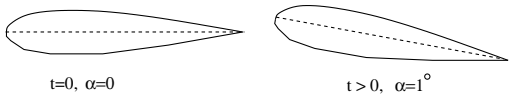


**a) Illustration of step change in angle of attack**

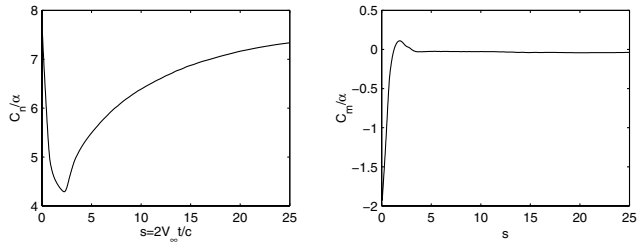


**b) Normal force and pitching moment responses for SC1095 airfoil ($M = 0.5$)**

**Fig. 3 Response to step change in angle of attack using field velocity approach.**

they are rescaled by the modified Jacobian. Thus, this approach presents a unique way of satisfying the GCL together with the use of the field velocity approach.

The requirement for evaluating the space and time metrics consistent with GCL is demonstrated in Sec. V. The problem studied for this case is the high speed forward flight case of a four bladed helicopter, which combines effects of blade deformation and vortex wake interaction.

## IV. Sample Results

### A. Step Change in Angle of Attack

Computations are performed to obtain responses of various airfoils to a step change in angle of attack using the field velocity approach. The indicial response is a combination of noncirculatory (wave propagation) and circulatory effects. For compressible flow, the noncirculatory component exponentially decays and the circulatory component grows to a final asymptotic value. A schematic of the problem is illustrated in Fig. 3a. Figure 3b shows the lift and pitching moment responses obtained from the CFD computations. The responses obtained from the CFD computations clearly show this trend. It is possible to obtain closed form analytical solutions to both the normal force and pitching moment responses for small times for a flat plate in linearized compressible flow [19]. The expressions of normal force and pitching moment coefficients are given by

$$\frac{C_n(s)}{\alpha} = \frac{4}{M}\left[1 - \frac{1-M}{2M}s\right]$$

$$\frac{C_m(s)}{\alpha} = \frac{1}{M}\left[1 - \frac{1-M}{2M}s + \left(1 - \frac{M}{2}\right)\frac{s^2}{2M}\right]$$

In these equations the quantity $s$ represents the nondimensional time, which is defined as the distance traveled by the airfoil in semichords. Figures 4a and 4b shows the comparison of the CFD results with the exact analytical solution for 4 different airfoils for the small nondimensional times (i.e., in the region the exact solution is valid). The results show good correlation with the exact solution for both lift and pitching moment. The correlation seems to degrade slightly with increasing thickness and camber. The NACA0006 airfoil, which is the closest to a flat plate approximation shows excellent correlation. On the other hand, the NACA0015 airfoil shows greater differences with the exact solution, especially at the higher Mach number.

A more detailed description and results of this approach for extracting indicial responses to build both linear and nonlinear kernels for reduced order aerodynamics models are documented in previous research efforts [20–22]. These reduced order models provide a powerful tool for aerodynamic load computations in active noise and vibration control studies [23,24].

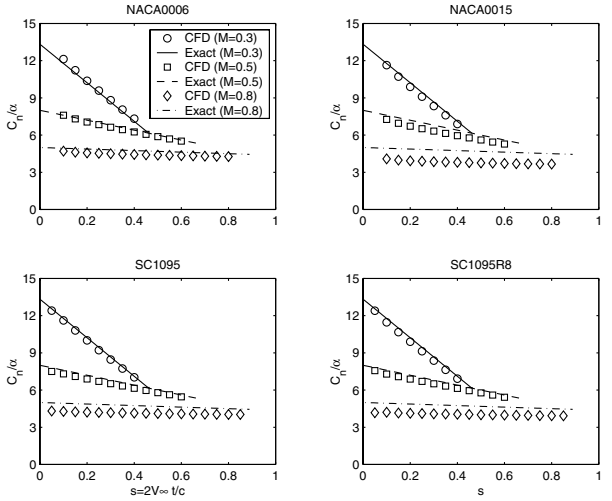


**a) CFD vs exact analytical (Normal force)**

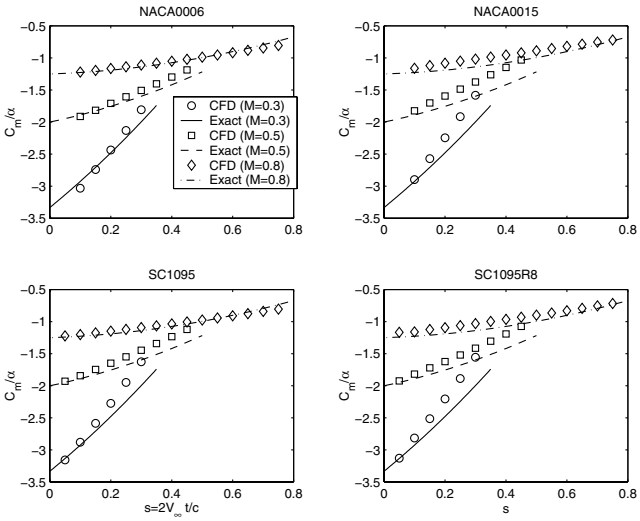


**b) CFD vs exact analytical (Pitching moment)**

**Fig. 4 Correlation between computed and exact analytical results for step change in angle of attack.**

### B. Interaction of an Airfoil with a Traveling Gust

The next unsteady flow problem studied is the aerodynamic response of an airfoil penetrating through a traveling vertical gust. The schematic of the problem is illustrated in Fig. 5a. The parameter that quantifies the relative convection speed of the gust is termed the gust speed ratio ($\lambda = V/(V + V_g)$, $V =$ free stream velocity, $V_g =$ gust convection speed).

The exact analytical solution for the response to a traveling vertical gust in compressible flow for small periods of time $0 \geq s \geq 2M/(1 + M)$ was developed using Evvard's [25] theorem and verified against Leishman's [26] results from the reverse flow theorem by Singh [27]. The exact analytical solutions are as follows:

$$C_l(s) = \frac{2s}{\sqrt{M\lambda^3}}\left[\frac{\lambda}{\lambda + (1-\lambda)M}\right]^{\frac{1}{2}} \tag{6}$$

$$C_{m_{le}}(s) = \frac{-s^2}{4\sqrt{M^3\lambda^2}}\left[\frac{\sqrt{2M + (1-M)\lambda}}{\lambda + (1-\lambda)M}\right] \tag{7}$$

Figure 5b shows the numerical prediction of the aerodynamic responses of an airfoil to a traveling vertical gust. The field velocity approach which was described earlier is used to implement the

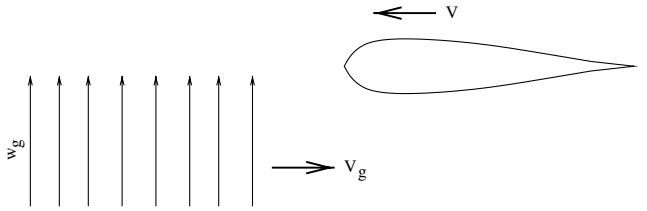


**a) Schematic of interaction with a vertical gust**

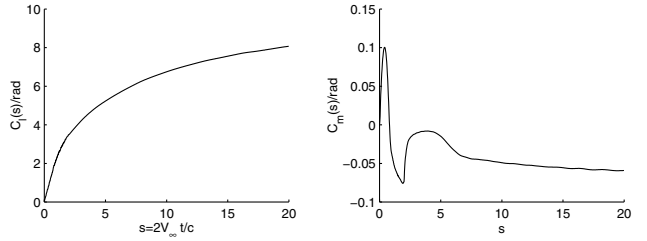


**b) Aerodynamic response to a vertical gust**

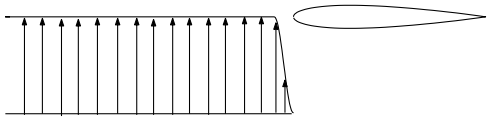

**c) Smooth edged gust used for simulation**

**Fig. 5 Response to a traveling vertical gust using field velocity approach.**

unsteady flow conditions for predicting the gust response. The effect of the gust is simulated by suitably modifying the field velocities in the vertical direction. At any instant of time the gust front can be calculated from the gust speed ratio. Thus, the field velocity values at all grid points behind the gust front are modified to be equal to the gust magnitude to simulate a propagating gust.

The initial flow conditions for the unsteady simulation is generated by obtaining a steady state flow solution around the airfoil. Once the initial steady state is obtained, the gust is initiated 15 chords upstream of the airfoil and made to convect at the desired speed representing the gust speed ratio [$V_g = V(\lambda^{-1} - 1)$]. The instant of time $s = 0$ corresponds to the instant where the gust front meets the airfoil leading edge. If the gust front is not differentiable as in the case of a sharp edged gust, second order time accuracy cannot be formally restored for the time metric computation. A smooth gust front with a cosine smoothing over 1% chords is used to rectify this effect. Figure 5c presents the smoothed out gust front, the smoothing is exaggerated to 5% chord here just for illustration purposes. The use of a smooth gust front helps in maintaining the time accuracy while still remaining accurate in predicting the load characteristics of a sharp edged gust front.

For moving gusts the rate of increase of the normal force is larger for the faster moving gusts. This is because of the acceleration effects associated with the impulsive change in the velocity field over a portion of the airfoil. This additional lift, which is the noncirculatory lift, decays rapidly and thereafter the total circulatory lift builds up slowly toward the steady state. The steady state magnitude is the same for all cases and is determined by the effective angle of attack caused by the vertical gust velocity. In the limiting case of infinite gust propagation speeds, the lift response corresponds to an indicial change in the angle of attack of equivalent magnitude (Wagner [28] problem). The case of zero gust speed or penetration of the airfoil into a stationary vertical gust is called the Küssner [29] problem.

The comparison of numerical solutions and exact solutions for four different gust speeds are presented in Figs. 6a and 6b. The numerical solutions show excellent correlation with exact analytical

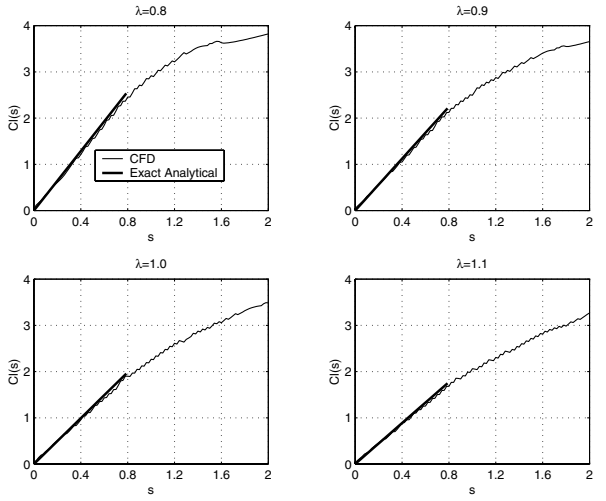


**a) Lift coeffcient**

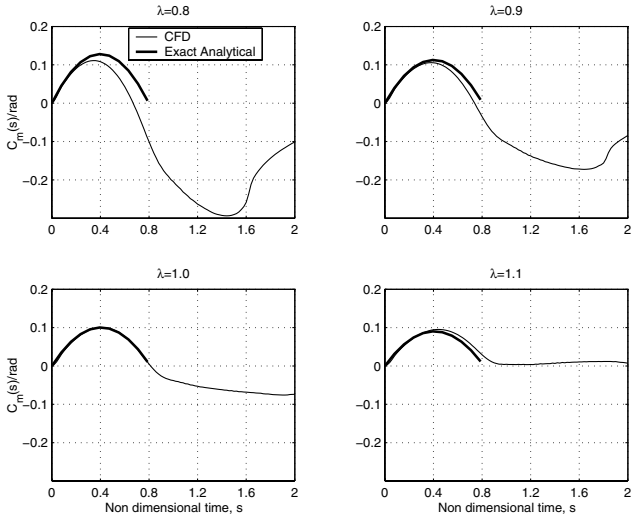


**b) Pitching moment**

**Fig. 6 Correlation between computed and exact analytical results for interaction of an airfoil with a traveling gust ($M = 0.6$).**

results especially for the stationary gust case ($\lambda = 1$); for the faster and slower convecting gust cases there are some deviations from the exact solution.

### C. Airfoil Vortex Interaction

An airfoil vortex interaction is an unsteady two dimensional problem in which a vortex convects perpendicular to the vorticity vector and influences the flow around an airfoil (Fig. 7a). It is the 2-dimensional equivalent of the parallel blade vortex interaction phenomenon observed in helicopter flight. Blade vortex interaction (BVI) is one of the loudest and most annoying sources of the rotor noise. The BVI noise propagates out of plane, usually forward and down, making it the most audible helicopter noise to an observer on the ground.

The aerodynamic generating mechanism of BVI noise can be explained briefly as follows: When the vortex is upstream of the blade it induces a downwash, and after the vortex passes by the blade an upwash is induced. The time varying vertical velocity change produced during the passage of the vortex changes the local angle of attack and causes a corresponding fluctuation in the blade loading. Thus, a sharp impulsive noise signature is created by the large rate of change of loading with time.

There are various ways of simulating the airfoil vortex interaction. One of the popular methodologies is called the perturbation approach

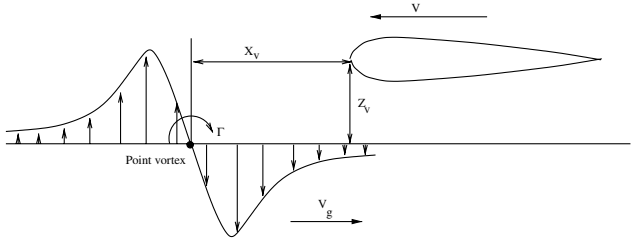


**a) Schematic of Airfoil Vortex Interaction**

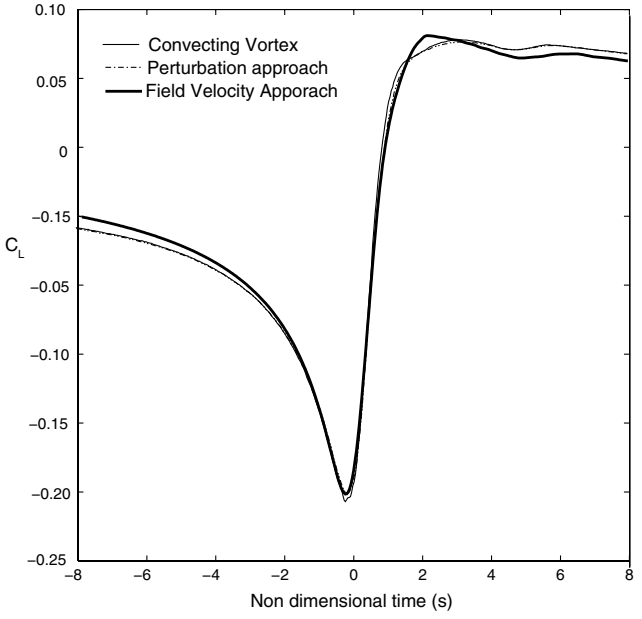


**b) Blade Loading time history ($M = 0.6$, miss distance [$Z_v$ = -0.25c)]**

**Fig. 7 Airfoil vortex interaction problem.**

[30], in which a flow field is decomposed into two parts despite nonlinearity: one is a prescribed vortical disturbance known to satisfy the governing equations, and the other obtained from the solution of the governing equations. As a result, the vortex structure is free of numerical diffusion. The second methodology is to use an accurate vortex-preserving Euler/Navier–Stokes solver [31], in which the vortex solution is computed directly from the numerical solution of the governing partial differential equations. This methodology requires a high resolution grid to prevent excessive numerical dissipation. The field velocity approach discussed earlier provides yet another methodology for simulating this problem. The grid time metrics are modified to include the velocity field induced by the vortex.

The results of the aerodynamic loads obtained from all three methodologies are presented in Fig. 7b. All three computations were performed on a C–H mesh (baseline mesh $= 217 \times 91$). For the vortex-preserving methodology, a higher resolution mesh (four time larger than baseline) is used. The mesh is also dynamically adapted at the regions in the neighborhood of the moving vortex to prevent excessive numerical diffusion [31]. It can be observed that the results from all the three approaches are in good agreement with each other. The field velocity approach presents a computationally efficient way of simulating this problem, as it does not require a high resolution grid and is computationally less complex compared with the perturbation approach.

### D. Aerodynamics and Acoustics in Low Speed Helicopter Forward Flight

Simulation of a real helicopter rotor blade in forward flight, as mentioned earlier, requires the use of the field velocity approach to prescribe the effects of the trailed vortex wake from the other rotor blades. The rotor blade motions which consists of pitch, flap and lag also need to be included.

The trailed vortex wake geometry can be obtained using a prescribed empirical formulas [32] or can be computed using a free wake analysis using a Lagrangian vortex lattice method [8]. The vortex wake geometry obtained consists of a description of the locus of the vortex filaments in space at discrete azimuthal positions of the rotor blade. Oftentimes, the azimuthal discretization of the wake geometry is much coarser ($\Delta\psi = 5^o$) than the azimuthal discretization used for the flow computations ($\Delta\psi = 0.25^o$). This necessitates the use of an appropriate interpolation technique to obtain the vortex wake geometries at the finer discretization level. In this case, the interpolation is performed spectrally, taking into advantage the periodicity of the wake with azimuthal angle.

The field velocity approach requires the evaluation of induced velocities caused by the vortex wake system at every grid point in the computational domain. This increases the computational complexity of the problem, as it is a $\mathcal{O}(M * N)$ computation, where $M$ is the number of vortex filaments and $N$ is the number of grid points. For a typical computation, there would be a need to compute induced velocities caused by about 1000 vortex filaments at each of the million grid points used at each time step. The increased computational complexity undermines the practicality of this approach. Therefore, a performance enhancement technique which maintains the necessary accuracy is required to perform routine computations using this methodology.

The performance enhancement is obtained using fast hierarchical algorithms [33,34]. Briefly, these algorithms use the recursive subdivision of the computational domain and a delineation of the near-field and far-field regions. Hence, for any grid point, the influence because of all the vortex filaments in its near field is evaluated exactly, whereas the effects of vortex filaments in the far field are evaluated using an appropriate interpolation or multipole expansion of the far-field potential.

The divide and conquer algorithm used is summarized in the schematic Fig. 8. It can be briefly described as follows:

The first stage involves initialization and preprocessing which are

1) *Geometric partitioning*: A box which encloses the grid is devised (level 0). This box is recursively subdivided in to smaller boxes (finer and finer levels).

2) *Local expansion*: The multipole expansion of all the vortex filaments (termed R expansion) about the center of the level 0 box due to all the vortex filaments which lie outside the limits of the level 0 box is evaluated (Fig. 8).

3) *Far-field expansion*: The number of vortices in each box are identified and the outer expansion for all boxes in all levels are evaluated.

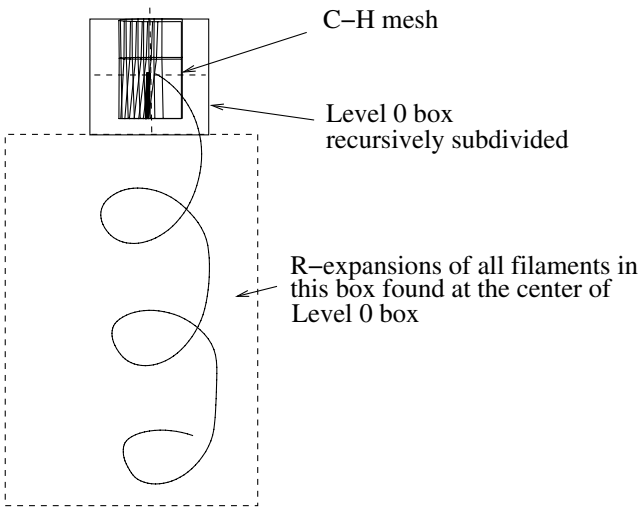


**Fig. 8 Schematic of the divide and conquer approach.**

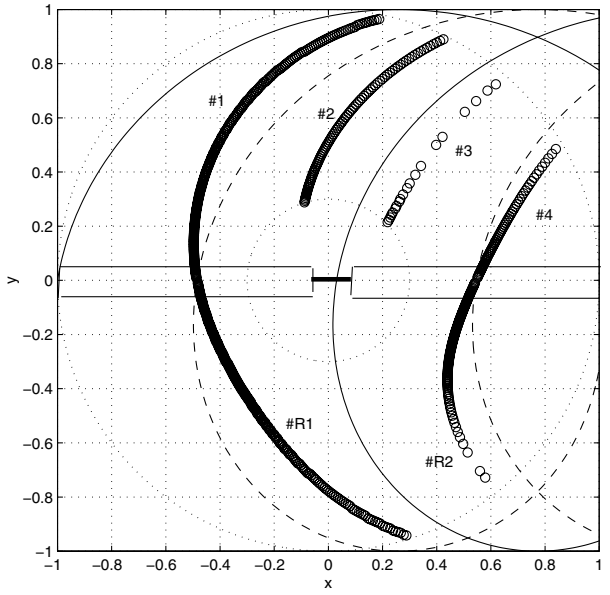


**a) BVI locations**

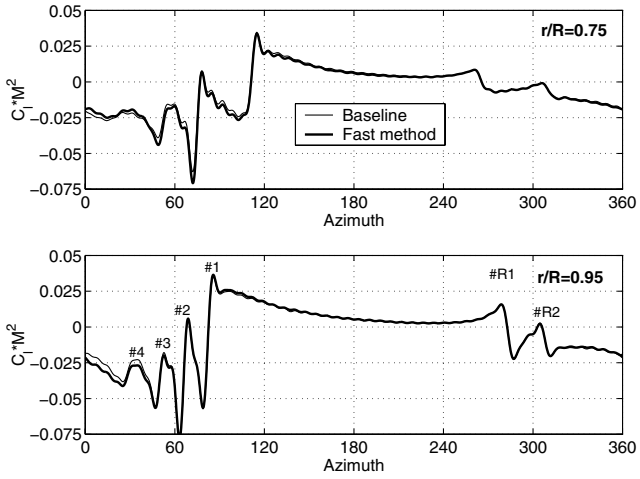


**b) Computed lift vs azimuth**

**Fig. 9 BVI problem for the OLS rotor ($\mu = 0.164$, $C_T = 0.00664$).**

Now the computations are performed for each grid point as follows:

1) The box in the finest level which contains the current grid point is found.

2) The Biot–Savart kernel is evaluated for all the vortex filaments in the particular box and its nearest neighbors.

3) The velocity because of far-field vortices is evaluated using outer expansions of boxes at coarser levels. Larger boxes are used as the distance between the evaluation points and vortex increases. In other words, vortex filaments are grouped together as one multipole expansion; the arger the distance, the larger volume that can be grouped as a single multipole expansion.

**Table 1 Wall clock times for Fast method compared with baseline for one revolution of the rotor ($d\psi = 0.25$ deg), $M$ = number of mesh points, $N$ = number of vortex filaments. (All computations performed on a 3.2 GHz Intel Xeon processor.)**

| Approach | $M$ | $N$ | Wall clock time |
|---|---|---|---|
| Baseline | 940,000 | 900 | 76 h |
| Fast | 940,000 | 900 | 9 h |

4) The velocity due to the vortex filaments outside the level 0 box is computed using the local expansion about the center of level 0 box that was calculated in the preprocessing step.

Figure 9b shows the lift time history obtained for the BVI problem shown in Fig. 9a. Here, the vortex wake geometry was obtained from a Lagrangian free wake analysis [8] and included in the CFD solver [11] using field velocity approach. The grid sizes and cpu time taken for the baseline and fast simulations are shown in Table 1. It is evident from these results that the algorithm presents a very efficient approach with little loss in accuracy.

The aerodynamic lift in Fig. 9b is obtained by simulating the same conditions as the wind tunnel experiments conducted by Splettstoesser et al. [35]. The experiments were conducted for a scaled AH-1 [operations load survey (OLS)] rotor with a tip Mach number of 0.664 and an advance ratio (ratio of free stream to tip Mach number) of 0.164. Also, the rotor plane is tilted at an angle of 1 deg backward from the free stream direction. Rigid blade motions (pitch and flap) that are consistent with the experiment are included in the flow computations. The BVI locations for such a flight condition is shown in Fig. 9a. These locations are found using the empirical definition of the vortex wake. It is evident from Fig. 9b that all the BVI hot spots are well captured by the CFD simulation.

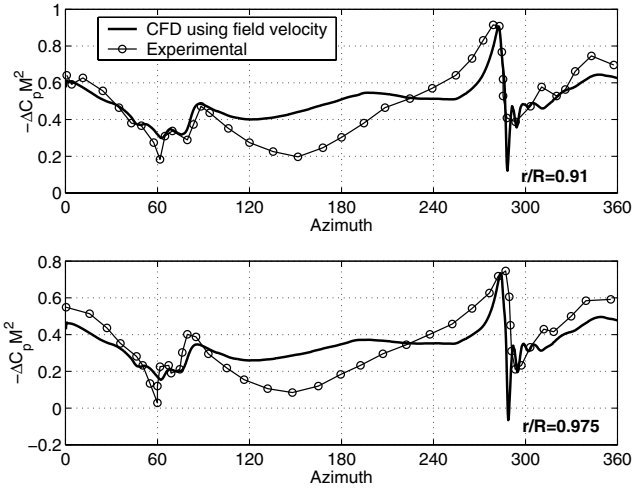


**a) Differential blade surface pressures at ($\frac{x}{c} = 0.03$) at two radial stations**

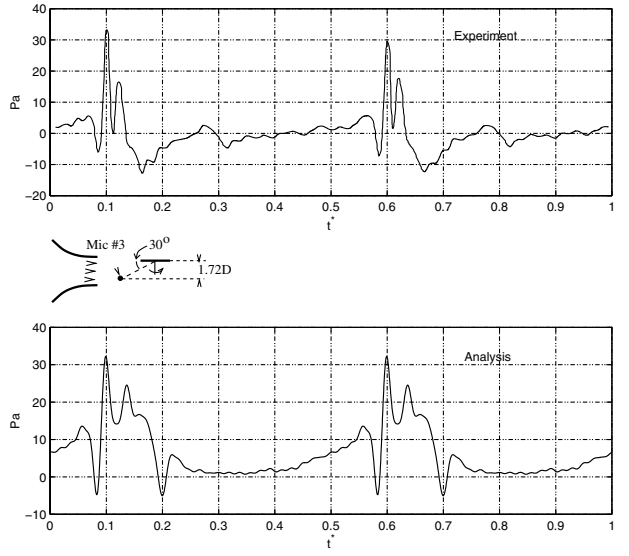


**b) OLS acoustic pressure time history at microphone #3**

**Fig. 10 Validation of aerodynamics and acoustics for the BVI problem for the OLS rotor ($\mu = 0.164$, $C_T = 0.00664$).**

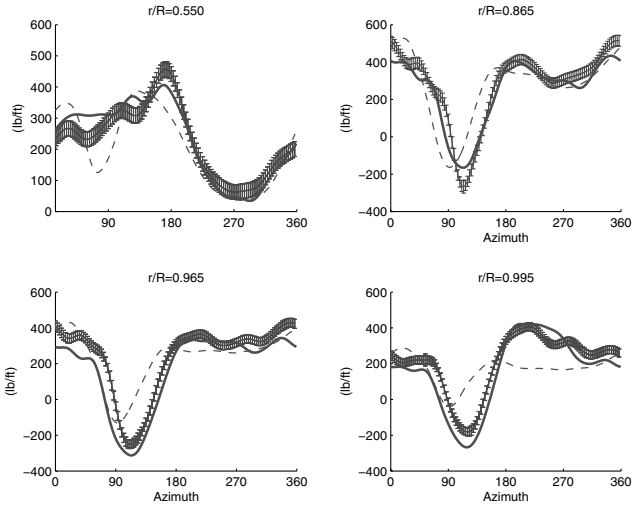


**a) Sectional normal forces at 4 radial stations**

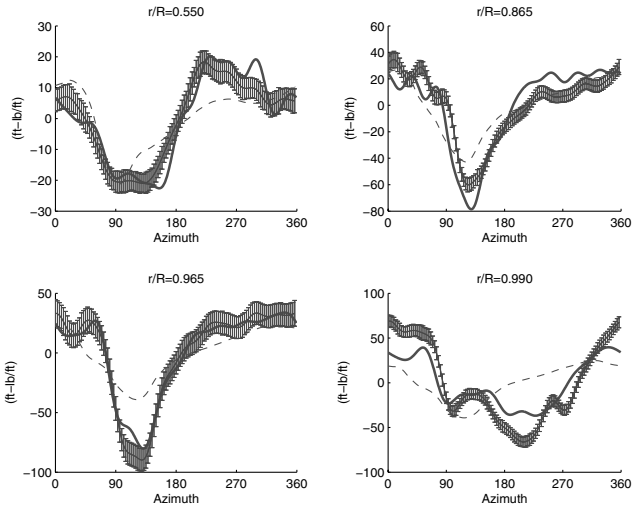


**b) Sectional pitching moments at 4 radial stations**

**Fig. 11 Predicted sectional aerodynamic loads for UH–60A Blackhawk, $V = 155$ kts, $(C_w/\sigma) = 0.0783$ (error bars = flight test data, solid line = CFD with field velocity approach, dashed line= lifting line aerodynamics).**

Figure 10a shows the differential blade surface pressure variation close to the leading edge ($x/c = 0.03$) predicted by CFD analysis as compared with the experimental measurements by Splettstoesser et al. [35]. The analysis gives fair correlation with the major features observed in the experiment. This is not unexpected for such a challenging problem. The phase of the impulsive loadings are captured. However, there are differences in the pressure derivatives, especially in the retreating side. The acoustic sound pressure levels are very sensitive to the rate of change of pressure (pressure derivatives). The blade surface pressures obtained from the CFD analysis were used to find the acoustic pressures at a specific microphone location (placed in front of the rotor at 30 deg out of plane and a distance of 1.72 rotor diameter below). The sound pressure level was computed using the acoustic prediction code WOPWOP [36] which solves the linearized Ffowcs–Williams–Hawkings equations [37] in observer time. The differences in the lift derivatives are reflected in the correlation of acoustic sound pressure levels, which show only fair agreement with the experimental data. However, the analysis does give very good prediction of the peak pressure, which determines the noise level in a dB scale.

A direct CFD computation using full wake capturing for analyzing this problem (i.e., without the use of field velocity approach) is very computationally intensive. A BVI dominated problem would require the vortex wake to be preserved at least for 2 revolutions. To minimize numerical diffusion and maintain the vortex structure for two revolutions at least 20 grid points are required across the vortex core at each section. This necessitates a large number of mesh points (of order $100 \times 10^6$) to model the entire flow field. In contrast, the field velocity approach used here provides a reasonable solution using just about a million mesh points at a very feasible computational cost.

### E. High Speed Forward Flight Case for the UH–60A (Blackhawk)

The high speed forward flight case combines the effects of transonic flow on the advancing side, large elastic deformations and wake effects caused by presence of negative lift. The effect of far wake becomes relatively less important compared with the previous case as the trailed wake is swept farther away from the rotor plane owing to the higher free stream velocity.

The flight conditions chosen for the results shown is that of the UH–60A helicopter in high speed forward flight with $V = 155$ kts and a thrust level $C_T = 0.00666$. This particular test case was chosen because of the well known modeling issues such as phase error in the negative lift and error in the peak to peak magnitudes of predicted pitching moments (Bousman [38]). Also flight test data (Kufeld et al.

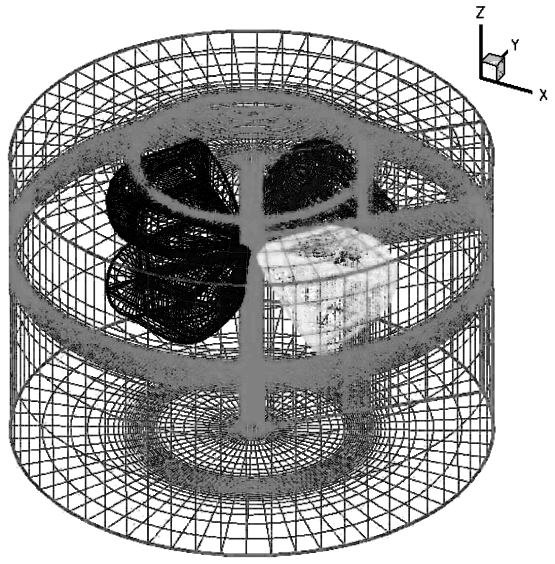


**a) Wake capturing meshes**

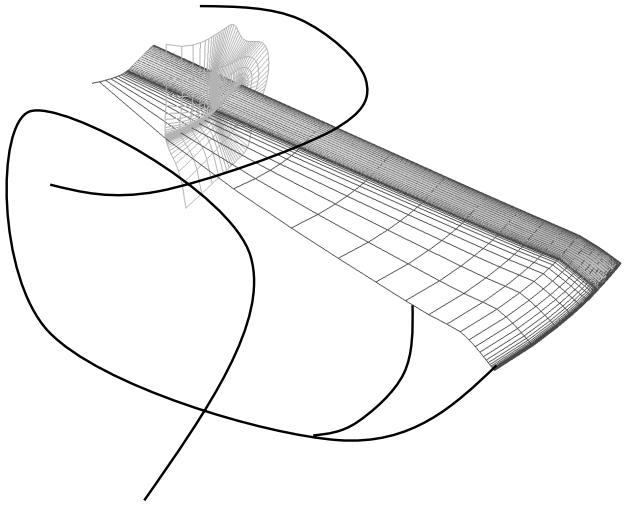

**b) Blade meshes and wake geometry**

**Fig. 12 Mesh topology for wake capturing methodology and field velocity approach.**

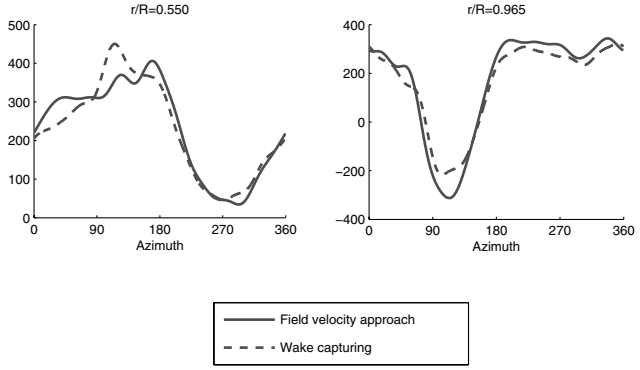


**a) Sectional normal forces at two radial stations**

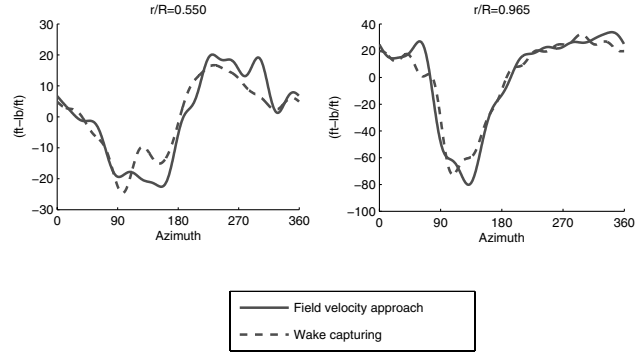


**b) Sectional pitching moment at 2 radial stations**

**Fig. 13 Sectional aerodynamic loads comparison of field velocity approach and wake capturing approach for UH–60A Blackhawk, $V = 155$ kts, $(C_w/\sigma) = 0.0783$.**

[39]) is available for this case to validate the numerical solutions computed. Recently an error was detected in the post processing of this experimental data and the flight test data and the error bars were revised [40].

The results for the present case is computed as a coupled aeroelastic solution. The solution also satisfies the trim condition of the aircraft. This is achieved by consistently coupling the CFD methodology with a comprehensive structural analysis code and free-wake analysis. The details of this approach can be found in [41–44].

There are two key physical mechanisms that dictate the waveform of sectional aerodynamic loads for the high speed forward flight conditions. They are a) transonic effects on the advancing side (tip Mach number on advancing side = 0.87) and b) interaction of wake vortices shed from the preceding blade. The negative lift on the advancing side causes the formation of a strong inboard vortex sheet which interacts with the following blade.

Figures 11a and 11b demonstrate the improved aerodynamic prediction capability of the present approach compared with the table lookup based linearized aerodynamic prediction schemes used in comprehensive rotorcraft aeroelastic analysis. Figure 11a shows the sectional normal forces at 4 radial stations. It can be seen that the CFD approach improves both the phase and magnitude of the predicted aerodynamic loads. The improvement is primarily because of the more accurate modeling of the transonic effects and wake interaction effects on the advancing side.

The wake interaction effects in the high speed forward flight are more benign compared with the low speed flight condition. Most of the aerodynamic loading effects can be captured by accurately resolving the vortex wake up to about 90 deg of wake age (half a revolution). Therefore a direct wake capturing CFD solution is feasible for this case. The wake capturing approach is a competing method for rotor aerodynamic load calculations and hence can serve as a platform for comparing the performance of the field velocity approach. The current approach [43] for wake capturing uses an overset mesh system which employs four blade meshes with $0.8 \times 10^6$ mesh points each that are immersed in a cylindrical background mesh with $2 \times 10^6$ mesh points (Fig. 12).

Figures 13a and 13b show the computed normal forces and pitching moments using the field velocity approach and the direct wake capturing approach. The methodologies show similar prediction trends and captures the phase and magnitude of the waveforms quite accurately compared with the flight test data (Figs. 11a and 11b). The wake capturing approach required almost 6 times more time compared with the field velocity approach for obtaining a solution with reasonable accuracy (Table 2). This is primarily because the wake capturing approach requires about

**Table 2 Wall clock times for field velocity approach compared with wake capturing approach for one revolution of the rotor at $d\psi = 0.5$ deg. (All computations performed on a 3.2 GHz Intel Xeon processor.)**

| Approach | mesh points | Wall clock time | Time per grid pt/ revolution |
|---|---|---|---|
| Field velocity approach | $0.8 \times 10^6$ | 6.5 h | 28.8 ms |
| Wake capturing | $5.2 \times 10^6$ | 37.5 h | 25.92 ms |

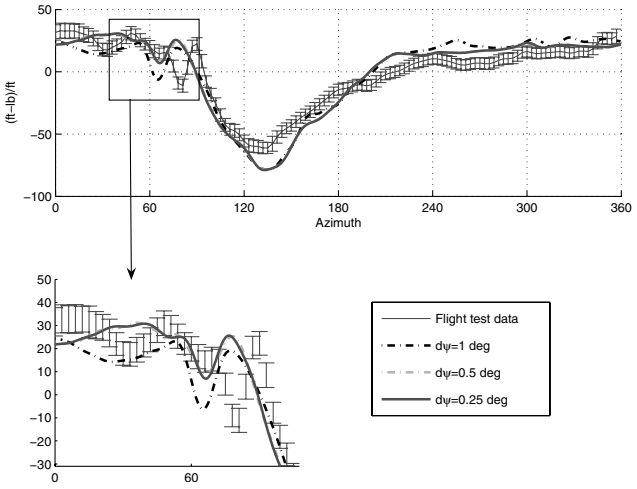


**a) With consistent time metric calculation**

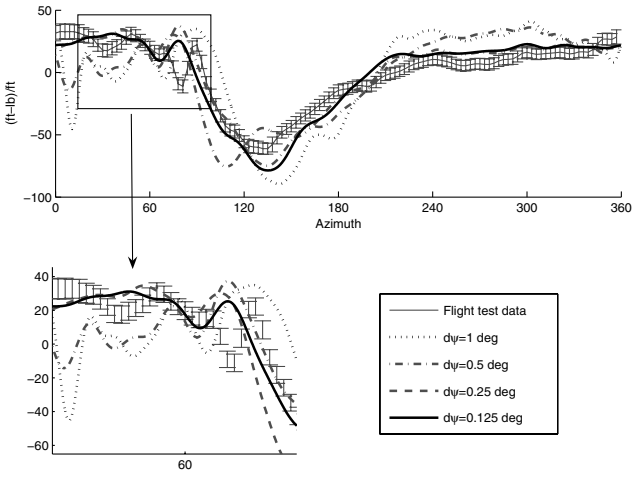


**b) Without consistent time metric calculation**

**Fig. 14 Time step dependence study of sectional pitching moments at $r/R = 0.865$ (UH–60A, $V = 155$ kts, $C_w/\sigma = 0.0783$).**

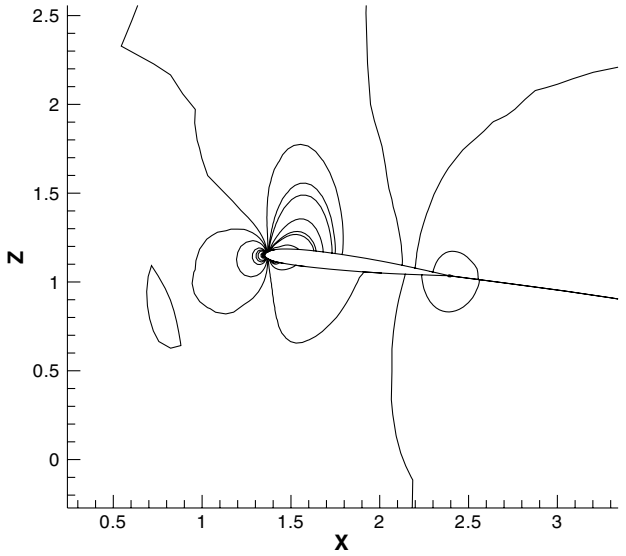


**a) Without consistent time metric calculation**

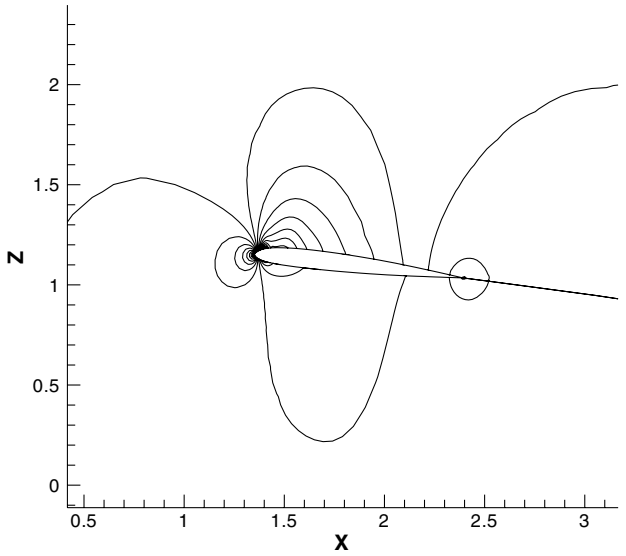


**b) With consistent time metric calculation**

**Fig. 15 Contours of pressure at $r/R = 0.965$ and azimuth $= 45$ deg (UH–60A, $V = 155$ kts, $C_w/\sigma = 0.0783$).**

6 times larger number of mesh points to model the entire rotor system whereas the field velocity approach models only one rotor blade. The time taken per grid point per revolution is larger for the field velocity approach because of the additional computational overhead for the induced velocity evaluation. However, the smaller number of grid points used mitigates this performance disadvantage.

## V. Necessity for Rigorously Enforcing GCL

A time step dependence study was performed for the high speed forward flight test case. The grid used for this study contained $0.8 \times 10^6$ mesh points. Figure 14a shows the variation of sectional pitching moments at an outboard radial station for the various time steps chosen. All the results that are presented in Fig. 14a used the evaluation of time metrics consistent with the GCL as discussed in the methodology section. It is evident that the solution is time converged at an azimuthal step of 0.25 deg. In Fig. 14b, results from the computations that did not use consistent evaluation of time metrics are illustrated. The waveforms of the pitching moment show large time step dependence in this case. The solutions are not time converged even at an azimuthal step of 0.125 deg.

Spurious source terms are generated when the GCL is not rigorously satisfied. This is the reason for the unphysical oscillations that are observed in Fig. 14b. These oscillations degrade the time accuracy of the solution procedure. The pressure contours presented in Figs. 15a and 15b further elucidate the presence of spurious sources in the absence of rigorous GCL enforcement. The pressure contours are much smoother when the time metrics are consistently evaluated.

The observations from the time dependence study strongly suggests that the consistent evaluation of time metrics for satisfying the GCL is critical for obtaining smooth time accurate solutions.

## VI. Concluding Remarks

This paper reviews a unique methodology for computing unsteady flow, namely the field velocity approach. A technique developed for rigorously satisfying the geometric conservation law when using deforming meshes together with the field velocity approach is also described. Computations of cell volumes and space metrics to a fourth order accuracy and consistent evaluation of time metrics for obtaining a conservative solution are discussed. Results presented include representative two-dimensional calculations for validating and evaluating the merits of the field velocity approach. Results for more complex realistic problems such as prediction of aerodynamics and acoustics of helicopter rotors in forward flight are also presented.

The following are the major conclusion drawn from this study:

1) The field velocity approach is found to be an accurate and efficient way for modeling unsteady flow problems. The results from the computations using field velocity approach show good correlation with both exact analytical results (2-D cases) and experimental data (3-D cases).

2) It was found that rigorously satisfying the geometric conservation law is required for problems which have large grid deformations and/or large changes introduced in the time metrics because of the field velocity approach.

## References

[1] Paramesvaran, V., and Baeder, J. D., "Indicial Aerodynamics in Compressible Flow: Direct Computational Fluid Dynamic Calculations," *Journal of Aircraft*, Vol. 34, No. 1, 1997, pp. 131–133.

[2] Singh, R., and Baeder, J., D., "On the Significance of Transonic Effects on Aerodynamics and Acoustics of Blade Vortex Interaction," AIAA Paper 96-1697, 1996.

[3] Sitaraman, J., and Baeder, J., D., "Enhanced Unsteady Airload Model Using CFD," AIAA Paper 2000-2465, Denver, Colorado, June 2000.

[4] Thomas, P. D., and Lombard, C. K., "Geometric Conservation Law and Its Application to Flow Computations on Moving Grids," *AIAA Journal*, Vol. 17, No. 10, 1979, pp. 1030–1037.

[5] Zhang, H., Reggio, M., Trepanier J. Y., and Camarero, R., "Discrete Form of the GCL for Moving Meshes and Its Implementation in CFD Schemes," *Computers and Fluids*, Vol. 22, No. 1, 1993, pp. 9–23.

[6] Demirdzic, I., and Peric, M., "Space Conservation Law in Finite Volume Calculations of Fluid Flow," *International Journal for Numerical Methods in Fluids*, Vol. 8, No. 9, 1988, pp. 1037–1050.

[7] Vinokur, M., "An Analysis of Finite-Difference and Finite-Volume Formulations for Conservation Laws," *Journal of Computational Physics*, Vol. 81, No. 1, 1989, pp. 1–52.

[8] Bagai, A., and Leishman, J. G., "The Maryland Free-Wake Analysis: Theory, Implementation and User's Manual," University of Maryland, Department of Aerospace Engineering, Technical Report Prepared for NASA Langley Research Center, Aeroacousitics Branch, Fluid Mechanics and Acoustics Division, Contract No. 015-2685, December 1995.

[9] Sitaraman, J., Baeder, J. D., and Chopra, I., "Computational Fluid Dynamics Based Unsteady Aerodynamic Modeling for Comprehensive Rotor Aeroelastic Analysis," *Proceedings of the American Helicopter Society Aerodynamics and Test and Evaluation Technical Specialist Meeting*, 2002.

[10] Srinivasan, G. R., Baeder, J. D., Obayashi, S., and McCroskey, W. J., "Flowfield of a Lifting Rotor in Hover: A Navier–Stokes Simulation," *AIAA Journal*, Vol. 30, No. 10, 1992, pp. 2371–2378.

[11] Srinivasan, G. R., and Baeder, J. D., "TURNS: A Free Wake Euler/Navier–Stokes Numerical Method for Helicopter Rotors," *AIAA Journal*, Vol. 31, No. 5, 1993, pp. 959–962.
[12] Baeder, J. D., and Srinivasan, G. R., "Computational Aeroacoustics Study of Isolated Blade–Vortex Interaction Noise," *Proceedings of the American Helicopter Society Aeromechanics Specialists Conference*, 1994.
[13] Roe, P. L., "Approximate Riemann Solvers, Parametric Vectors, and Difference Schemes," *Journal of Computational Physics*, Vol. 43, No. 3, 1981, pp. 357–372.
[14] Vatsa, V. N., Thomas, J. L., and Wedan, B. W., "Navier–Stokes Computations of Prolate Spheroids at Angle of Attack," AIAA Paper 87-2627, Aug. 1987.
[15] Jameson, A., and Yoon, S., "Lower–Upper Implicit Schemes with Multiple Grids for the Euler Equations," *AIAA Journal*, Vol. 25, No. 7, 1987, pp. 929–935.
[16] Yoon, S., and Jameson, A., "An LU-SSOR Scheme for the Euler and Navier Stokes Equations," AIAA Paper 1987-0600, 1987.
[17] Pulliam, T., and Steger, J., "Implicit Finite Difference Simulations of Three Dimensional Compressible Flow," *AIAA Journal*, Vol. 18, No. 2, 1980, pp. 159–167.
[18] Hyunh, H. T., "Accurate Monotone Cubic Interpolation," *SIAM Journal on Numerical Analysis*, Vol. 30, No. 1, 1993, pp. 57–100.
[19] Lomax, H., "Indicial Aerodynamics," *AGARD Manual of Aeroelasticity: Part 2*, NATO, Advisory Group for Aerospace Research and Development, Nov. 1968, Chap. 6.
[20] Sitaraman, J., "Computational Fluid Dynamics Based Enhanced Indicial Aerodynamic Models," Master's Thesis, University of Maryland, College Park, MD, 2002.
[21] Singh, R., and Baeder, J. D., "The Direct Calculation of Indicial Lift Response of a Wing Using Computational Fluid Dynamics," *Journal of Aircraft*, Vol. 35, No. 4, 1997, pp. 465–471.
[22] Lee, D., Leishman, J. G., and Baeder, J. D., "A Nonlinear Indicial Method for Calculation of Unsteady Airloads," *Proceedings of the 59th Forum of the American Helicopter Society*, 2003.
[23] Roget, B., and Chopra, I., "Robust Individual Blade Control Algorithm for a Dissimilar Rotor," *Journal of Guidance, Control, and Dynamics*, Vol. 25, No. 5, 2002, pp. 915–923.
[24] Wang, B., Baeder, J. D., and Singh, R. K., "A Computational Study of Trailing-Edge Flap Aerodynamics and Acoustics," *Proceedings of the 55th Forum of the American Helicopter Society*, 1999.
[25] Evvard, J. C., "Use of Source Distribution for Evaluating Theoretical Aerodynamics of Thin Finite Wings at Supersonic Speeds," NACA, Rept. 951, 1950.
[26] Leishman, J. G., "Unsteady Aerodynamics of Airfoils Encountering Traveling Gusts and Vortices," *Journal of Aircraft*, Vol. 34, No. 6, 1997, pp. 719–729.
[27] Singh, R., "Transonic Effects on Aerodynamics and Acoustics of Blade–Vortex Interaction," Ph.D. Dissertation, University of Maryland, College Park, MD, 1999.
[28] Leishman, J. G., *Principles of Helicopter Aerodynamics*, Cambridge University Press, Cambridge, 2000.
[29] Küssner, H. G., "General Airfoil Theory," NASA TM 979, 1941.
[30] Srinivasan, G. R., and McCroskey, W. J., "Numerical Simulations of Unsteady Airfoil Vortex Interactions," *Vertica*, Vol. 11, No. 1-2, 1987, pp. 3–28.
[31] Tang, L., "Improved Euler Simulation of Helicopter Vortical Flows," Ph.D. Dissertation, University of Maryland, 1998.
[32] Beddoes, T. S., "A Wake Model for High Resolution Airloads," *Proceedings of the International Conference on Rotorcraft Basic Research*, 1985.
[33] Greengard, L., and Rokhlin, V., "A Fast Algorithm for Particle Simulations," *Journal of Computational Physics*, Vol. 73, No. 2, 1987, pp. 325–348.
[34] Barnes, J. E., and Hut, P., "A Hierarchical O(N log N) Force Calculation Algorithm," *Nature (London)*, Vol. 324, No. 4, 1986, pp. 446–449.
[35] Splettstoesser, W. R., Schultz, K. J., Boxwell, D. A., and Schmitz, F. H., "Helicopter Model Rotor-Blade Vortex Interaction Impulsive Noise: Scalability and Parametric Variations," *Proceedings of the 10th European Rotorcraft Forum*, 1984.
[36] Brentner, K. S., "Prediction of Helicopter Rotor Noise—A Computer Program Incorporating Realistic Blade Motions and Advanced Formulation," NASA TM 87721, 1986.
[37] Ffowcs Williams, J. E., and Hawkings, D. L., "Sound Generation by Turbulence and Surface in Arbitrary Motion," *Philosophical Transactions of the Royal Society of London, Series A: Mathematical and Physical Sciences*, Vol. 264, No. 1151, May 1969, pp. 321–342.
[38] Bousman, W. G., "Putting the Aero Back Into Aeroelasticty," *Eighth Army Research Office Workshop on Aeroelasticity of Rotorcraft Systems*, 1999.
[39] Bousman, G., Kufeld, R. M., Balough, D., Cross, J. L., Studebaker, K. F., and Jennison, C. D., "Flight Testing the UH–60A Airloads Aircraft," *50th Annual Forum of the American Helicopter Society*, 1994.
[40] Kufeld, R. M., and Bousman, W. G., "UH–60A Airloads Program Azimuth Reference Correction," Technical Note, *Journal of the American Helicopter Society*, Vol. 50, No. 2, 2005, pp. 211–213.
[41] Sitaraman, J., Baeder, J. D. and Chopra, I., "Validation of UH–60A Blade Aerodynamic Characteristics Using CFD," *Proceedings of the 59th Annual Forum of American Helicopter Society*, 2003.
[42] Datta, A., Sitaraman, J., Chopra., I, and Baeder, J., "Analysis Refinements for Prediction of Rotor Vibratory Loads in High-Speed Forward Flight," *American Helicopter Society 60th Annual Forum*, 2004.
[43] Sitaraman, J., Datta, A., Chopra., I., and Baeder, J., "Coupled CFD/CSD Prediction of Rotor Aerodynamic and Structural Dynamic Loads for Three Critical Flight Conditions," *Proceedings of the 31st European Rotorcraft Forum*, 2005.
[44] Potsdam, M., Yeo, H., and Johnson, W., "Rotor Airloads Prediction Using Loose Aerodynamic/Structural Coupling," *Presented at the American Helicopter Society 60th Annual Forum*, 2004.

K. Ghia
*Associate Editor*